PHYSICAL REVIEW B VOLUME 28, NUMBER 2 15 JULY 1983

Lithium-intercalated graphite: Self-consistent electronic structure for stages one, two, and three

N. A. W. Holzwarth*
Corporate Research—Sciences Laboratory, Exxon Research and Engineering Company, P. O. Box 45, Linden, New Jersey 07036

Steven G. Louie
Department of Physics, University of California, Berkeley, California 94720

Sohrab Rabii
Moore School of Electrical Engineering, University of Pennsylvania, Philadelphia, Pennsylvania 19104
(Received 23 February 1983)

First-principles electronic structure calculations were carried out for LiC_6, LiC_{12}, and LiC_{18} representing first-, second-, and third-stage model graphite intercalation compounds. By comparing the charge density of these compounds to that of reference graphite compounds, we could define a "total difference density" in order to quantify charge transfer and polarization in these materials. The total difference density is found to be highly concentrated near the intercalant ions. However, the conduction electrons (those in partially occupied bands) are found to have the distribution of virtually undistorted π wave functions and have a much more delocalized distribution than that of the total difference density. These two types of charge distributions account for many of the unusual electronic properties of graphite intercalation compounds.

I. INTRODUCTION

In a recent short paper[1] we presented the results for the electronic structure of a model third-stage graphite intercalation compound: LiC_{18}. The present paper is a more detailed presentation of this work in comparison with results for the two lower-stage compounds, LiC_6 and LiC_{12}. Results for graphite itself and for diamond were presented in separate papers.[2]

The calculational methods are described in Ref. 2. Briefly, the calculations were carried out self-consistently in the local-density approximation using a pseudopotential formulation and by representing the electronic wave functions in terms of a mixed-basis set consisting of plane waves and linear combinations of atomic orbitals as developed by Louie, Ho, and Cohen.[3] The ionic pseudopotentials were generated from all-electron atomic calculations using the formulation of Hamann, Schlüter, and Chiang.[4] The exchange-correlation potential was that of Hedin and Lundqvist.[5] These calculational methods were particularly successful in determining a valence charge density of graphite which is in excellent agreement with that determined from experimental x-ray form factors.[6]

The outline of the paper is as follows. In Sec. II, the crystal structures chosen for this study are discussed. In Sec. III, the results of the charge-density distributions and local densities of states are presented. In Sec. IV, the energy bands and Fermi-surface properties are discussed. Discussion and conclusions are presented in Sec. V.

II. STRUCTURAL CONSIDERATIONS

Despite the fact that from a theoretical point of view the Li-intercalated graphite compounds are the most simple of the intercalation compounds,[7] they are apparently somewhat difficult to prepare and to characterize. Staged compounds of Li-intercalated graphite as high as stage five have been reported,[8] but the structure and stoichiometries of even the low-stage compounds are only recently being determined. In general, the Li atoms are inserted between two layers of graphite, causing the two layers to change their registry from *AB* stacking to *AA* stacking and causing a 10% increase in the interlayer separation from 3.35 to 3.70 Å.[9] The Li atoms are arranged directly between carbon hexagons in a triangular lattice having a $\sqrt{3}\times\sqrt{3}$ registry with respect to the hexagonal lattice of graphite. The intralayer lattice constant of the hexagonal graphite lattice constant a is also slightly dilated with respect to that of graphite. For the first-stage compounds, the intralayer dilation is 1% and $a=2.485$ Å.[9] For higher-stage compound the dilation is somewhat less. For simplicity we chose to study the idealized stoichiometries and structures shown in Fig. 1 and detailed in Table I. Some of the reasoning behind these choices is given below.

The first-stage compound is agreed to have the stoichiometry LiC_6. Several authors[9–11] have suggested the structure of LiC_6 to be D_{6h}^1 symmetry with layer stacking $A\alpha A\alpha A\alpha$.[12] On the basis of electron diffraction, Kambe *et al.*[13] determined the low-temperature (<220 K) form of LiC_6 to have a layer stacking of $A\alpha A\beta A\gamma$. This structure is apparently in disagreement with neutron-diffraction results.[11] For the present study, we chose to use the simpler D_{6h}^1 structure, shown in Fig. 1 (first panel), in order to compare with our previous non-self-consistent calculations using modified Korringa-Kohn-Rostoker (KKR) techniques.[14,15]

The second-stage compound apparently has two metastable stoichiometries at room temperature: LiC_{12} and LiC_{18}.[8–11,16–18] Guérard and Hérold[9] suggested the structure to have the stacking sequence $AA\alpha AA\alpha AA\alpha AA\alpha$ which is in agreement with recent neutron-diffraction results for the LiC_{12} form of second-stage Li-intercalated

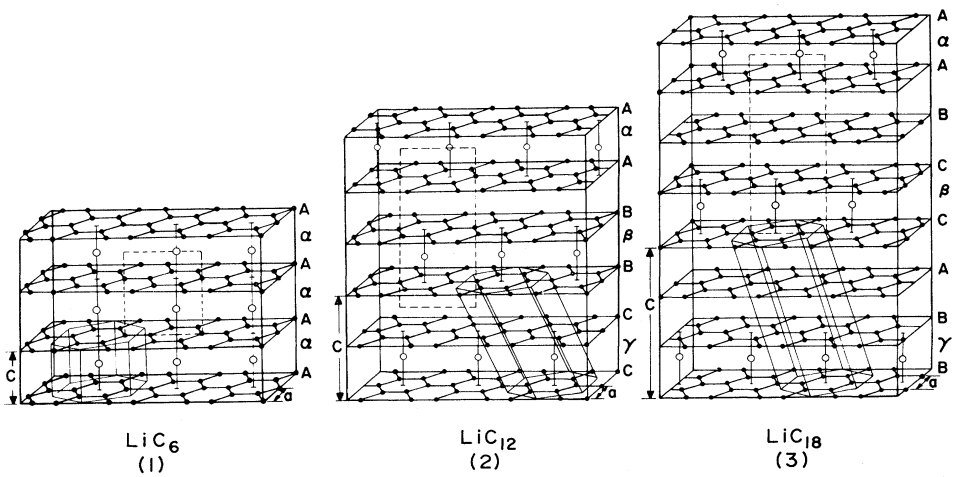

FIG. 1. Structures of Li-intercalated graphite compounds LiC_6 (stage 1), LiC_{12} (stage 2), and LiC_{18} (stage 3) assumed in present study. Carbon atoms are denoted by filled circles connected along nearest-neighbor bonds. Li atoms are denoted by unfilled circles. Primitive unit cells are indicated for each structure. Dashed rectangle in each structure denotes the plane used in contour plots shown in Figs. 2–7.

TABLE I. Lattice parameters for Li-intercalated graphite compounds.

LiC_6 (structure based on Ref. 9)

Primitive lattice vectors:

$\vec{T}_1=a\sqrt{3}[(\sqrt{3}/2)\hat{x}+\frac{1}{2}\hat{y}]$,

$\vec{T}_2=a\sqrt{3}[-(\sqrt{3}/2)\hat{x}+\frac{1}{2}\hat{y}]$,

$\vec{T}_3=c_1\hat{z}$, $a=2.485$ Å, $c_1=3.706$ Å

Atomic locations within unit cell:

C atoms: $\pm[\frac{1}{3}(\vec{T}_1+\vec{T}_2)+\frac{1}{2}\vec{T}_3]$

$\pm[\frac{1}{3}\vec{T}_1+\frac{1}{2}\vec{T}_3]$

$\pm[\frac{1}{3}\vec{T}_2+\frac{1}{2}\vec{T}_3]$

Li atom: 0

Symmetry directions:

$\Gamma\le k\le A$ $\quad\vec{k}=x\vec{G}_3$ $\quad 0\le x\le\frac{1}{2}$

$\Gamma\le k\le M$ $\quad\vec{k}=x(\vec{G}_1-\vec{G}_2)$ $\quad 0\le x\le\frac{1}{2}$

$\Gamma\le k\le K$ $\quad\vec{k}=x(\vec{G}_1+\vec{G}_2)$ $\quad 0\le x\le\frac{1}{3}$

LiC_{12} and LiC_{18} (assumed structures)

Primitive lattice vectors:

$\vec{T}_1=a\sqrt{3}[(\sqrt{3}/2)\hat{x}+\frac{1}{2}\hat{y}]$, $\vec{T}_2=a\sqrt{3}[-(\sqrt{3}/2)\hat{x}+\frac{1}{2}\hat{y}]$,

$\vec{T}_3=(2a/\sqrt{3})\hat{y}+c_n\hat{z}$, $a=2.485$ Å,

$c_2=7.056$ Å(LiC_{12}), $c_3\equiv 10.406$ Å(LiC_{18})

LiC_{12} and LiC_{18} (assumed structures *continued*)

Atomic locations within unit cells:

C atoms: $\pm\left[\left(\frac{1-2p_n}{3}\right)(\vec{T}_1+\vec{T}_2)+p_n\vec{T}_3\right]$

$\pm\left[\left(\frac{1-2p_n}{3}\right)\vec{T}_1-\frac{2p_n}{3}\vec{T}_2+p_n\vec{T}_3\right]$

$\pm\left[\frac{-2p_n}{3}\vec{T}_1-\left(\frac{1+2p_n}{3}\right)\vec{T}_2+p_n\vec{T}_3\right]$

$\pm\left[-\left(\frac{1+2p_n}{3}\right)(\vec{T}_1+\vec{T}_2)+p_n\vec{T}_3\right]$

$\pm\left[-\left(\frac{1+2p_n}{3}\right)\vec{T}_1-\frac{2p_n}{3}\vec{T}_2+p_n\vec{T}_3\right]$

$\pm\left[\frac{-2p_n}{3}\vec{T}_1+\left(\frac{1-2p_n}{3}\right)\vec{T}_2+p_n\vec{T}_3\right]$

$p_n\equiv\frac{c_1}{2c_n}$ where $n=2$ for LiC_{12} and 3 for LiC_{18}

Additional C atoms in LiC_{18}: $\pm[-\frac{1}{3}(\vec{T}_1+\vec{T}_2)+\frac{1}{2}\vec{T}_3]$

$\pm[-\frac{1}{3}\vec{T}_1+\frac{1}{2}\vec{T}_3]$

$\pm[+\frac{1}{3}\vec{T}_2+\frac{1}{2}\vec{T}_3]$

Li atom: 0

Symmetry directions:

$\Gamma\le k\le A$ $\quad\vec{k}=x\vec{G}_3$ $\quad 0\le x\le\frac{1}{2}$

$\Gamma\le k\le M$ $\quad\vec{k}=x(\vec{G}_1-\vec{G}_2)$ $\quad 0\le x\le\frac{1}{2}$

$\Gamma\le k\le\tilde{K}$ $\quad\vec{k}=x(\vec{G}_1+\vec{G}_2)$ $\quad 0\le x\le\frac{1}{3}$

graphite.[11,18] Recently, Woo *et al.*[18] have determined the second-stage LiC_{18} to have the stacking sequence *AB-BA-AB* with no in-plane order of the Li layers. For simplicity, we chose to study second-stage LiC_{12} in the hypothetical structure shown in Fig. 1 (second panel), having a stacking sequence $A\alpha AB\beta BC\gamma CA\alpha A$. Such a stacking sequence for the graphite layers has been observed in second-stage graphite nitrate[19] and in second-stage potassium graphite.[20] The stacking sequence for the Li layers was chosen in order to have a unit cell of only 13 atoms with an inversion center.

To our knowledge, the structure of the third-stage compound has not been reported. We assumed the stoichiometry LiC_{18} and chose the structure $A\alpha ABC\beta CAB\gamma BCA\alpha ABC\beta$ as shown in the third panel of Fig. 1 in order to have a unit cell of only 19 atoms with an inversion center and to maintain a reasonable local geometry for the C and Li atoms. The stacking sequence for the graphite layers is not what is commonly found for other third-stage compounds,[10,20] where the adjacent graphite layers order as *ABA* and *ACA*. The *ABC* stacking is that found in the less common form of graphite—rhombohedral graphite.[21,22] The structural difference between Bernal[23] and rhombohedral graphite has a large effect on the Fermi-surface properties of the two forms of graphite.[21,22] However, for LiC_{18}, the Fermi energy is much larger and subtle structural differences are not as important. One of the factors which establishes the charge distribution in LiC_{18} is the tendency of electrons to delocalize along the *c* axis, which depends upon the average number of nearest-neighbor atoms in adjacent layers and which is the same for the *ABC* and *ABA* stackings.

III. RESULT FOR ELECTRONIC DENSITY DISTRIBUTIONS

In Ref. 2 we showed that the present calculational methods yield a valence electronic charge density for graphite and diamond which are in excellent agreement with that inferred from x-ray-intensity measurements.[6] Since we have used the pseudopotential approximation, the density in the core region does not have exactly correct shape, but because of the norm-conserving aspect of the pseudopotential,[4] the integrated charge within the pseudopotential radius is equal to the actual charge within the same volume.

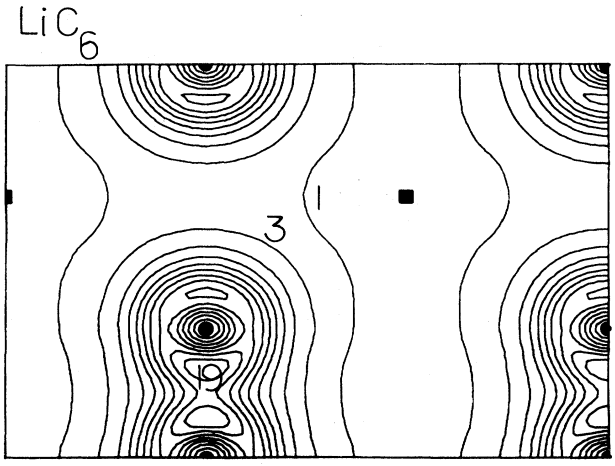

FIG. 2. Contour plot of total valence-electron charge density of LiC_6. Contour values are given in units of 0.1 electrons/Å^3. Atomic positions are denoted by filled squares for Li and circles for carbon. Plane shown contains *c* axis and passes through Li atoms and C—C bonds as shown by the dashed rectangle in Fig. 1 (first panel).

Results for the valence electronic charge density for LiC_6, LiC_{12}, and LiC_{18} are shown in Figs. 2—4, respectively. From these figures it is seen that the density distributions for the Li-intercalated graphite compounds are very similar to each other and to graphite itself. The 1% dilation of the intralayer lattice constant in the intercalation compounds results in a slightly lower peak density along a C—C bond than in graphite. Close examination of the density for LiC_6 in comparison to graphite itself reveals a slightly higher density in the π-orbital region. This excess π density is a direct consequence of the charge transfer from the Li intercalant ions. In LiC_{12} and near the bounding layer of LiC_{18}, this excess π density is seen to be asymmetric with higher density on the side facing another C layer than on the side facing a Li layer. This result seems counterintuitive since one expects the Li ions to polarize the graphite electrons toward the Li planes. However, the distance between C planes in the "sandwich region" on either side of a Li plane is 10% larger than the distance between adjacent C planes. This expansion tends to de-

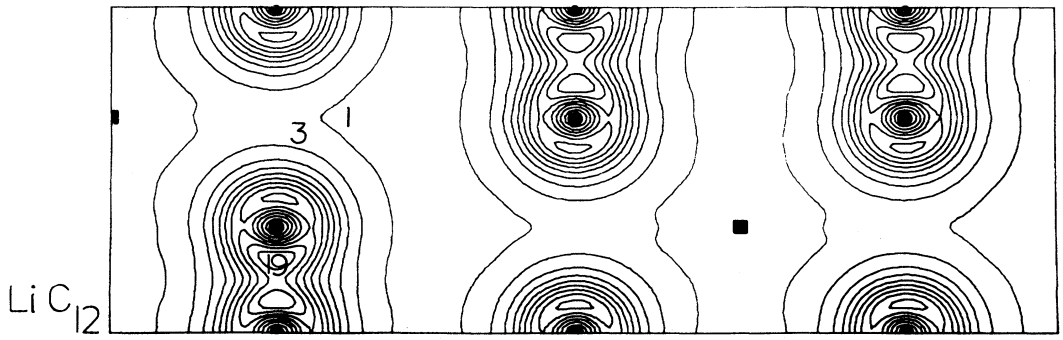

FIG. 3. Contour plot of total valence-electron charge density of LiC_{12}. Contour values are given in units of 0.1 electrons/Å^3. Atomic positions are denoted by filled squares for Li and circles for carbon. Plane shown contains *c* axis and passes through Li atoms and C—C bonds as shown by the dashed rectangle in Fig. 1 (second panel).

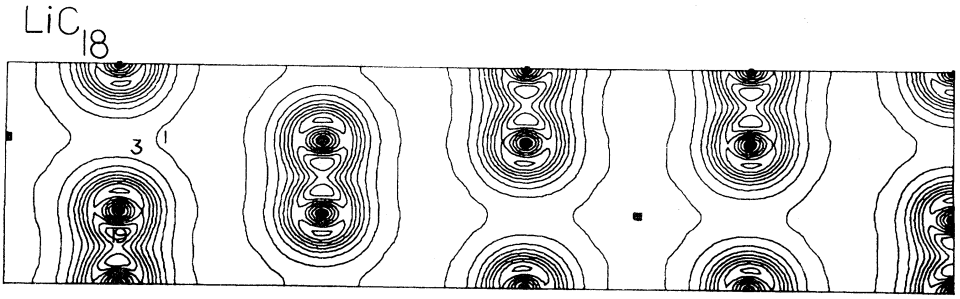

FIG. 4. Contour plot of total valence-electron charge density of LiC_{18}. Contour values are given in units of 0.1 electrons/Å^3. Atomic positions are denoted by filled squares for Li and circles for carbon. Plane shown contains c axis and passes through Li atoms and C—C bonds as shown by the dashed rectangle in Fig. 1 (third panel).

crease the valence-electron density between C planes on either side of a Li plane with respect to the density between adjacent C planes. The expansion effect masks the polarization effect, and the net result is the asymmetric distribution seen in Figs. 3 and 4.

In order to factor out the effects of c-axis expansion from the more interesting effects of charge transfer and polarization, we compared the density of each of the intercalation compounds with that of graphite modified to the same structures. For future reference, we will call these fictious modified graphite materials C_6,C_{12}, and C_{18} for the first-, second- and third-stage forms. The total-electron-difference density for LiC_6 is shown in Fig. 5(a). The peak density is located in π-like contours on each C site. These contours are distorted in the direction of the Li ions in evidence of the polarization effects. In order to better understand the origin of this structure, the total-electron-difference density was considered as a sum of two parts: the conduction-electron-difference contribution [Fig. 5(b)] and the valence-electron-difference contribution [Fig. 5(c)]. The conduction-electron-difference contribution was defined as that derived from the partially filled bands. This density represents states located in energy above E_F of pure graphite and corresponds to states receiving the transferred charge. These states determine the Fermi-surface properties of LiC_6. The valence-electron-difference contribution was defined as the difference between the total-difference density and the conduction-electron-difference contributions. It can be directly associated with the polarization of the graphite charge density. The total-difference density and the conduction-electron-difference density both integrate to a single electron per unit cell while the valence-electron-difference density integrates to no net charge per unit cell.

From Fig. 5(b), it is apparent that the conduction-electron-difference contribution retains its π-like form with very slight polarization effects. This result had been noted previously on the basis of non-self-consistent calculations.[15] By the argument to follow, the effect is expected to be a general property of graphite intercalation compounds due to the nature of the conduction states, especially their partially antibonding character.[15] From perturbation theory, the distortion polarizability of a graphite state depends largely on virtual excitations to the lowest unoccupied state of the compound. The wave function for this state is a smooth function in the layer plane and its matrix element with a wave function having oscillatory

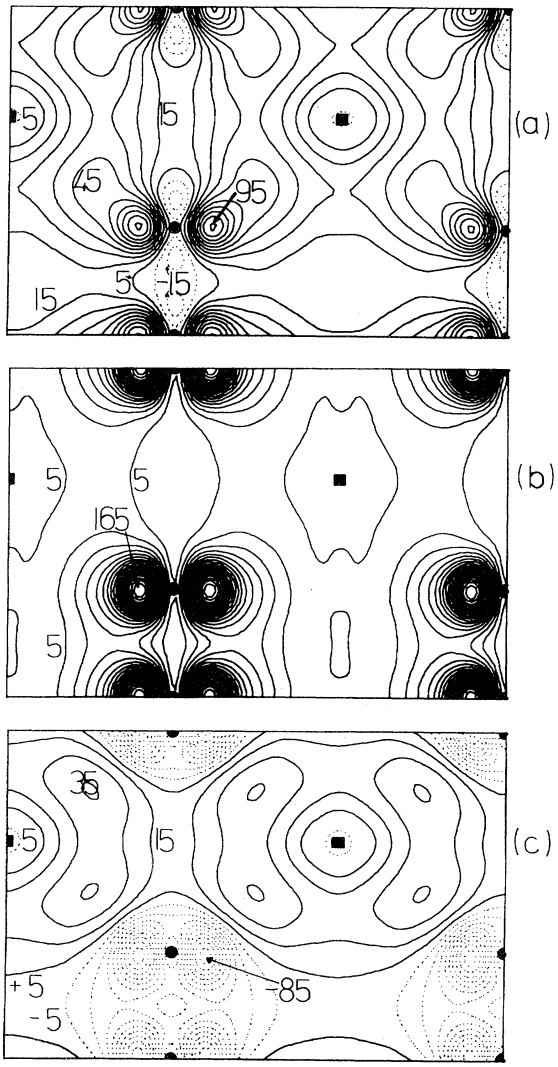

FIG. 5. Contour plots of electronic charge density for LiC_6: (a) total-difference density, (b) conduction-electron contribution, and (c) valence-electron contribution. Contour values are given in units of 0.001 electrons/Å^3. Atomic positions are denoted by filled squares for Li and circles for carbon. Plane shown is the same as in Fig. 2.

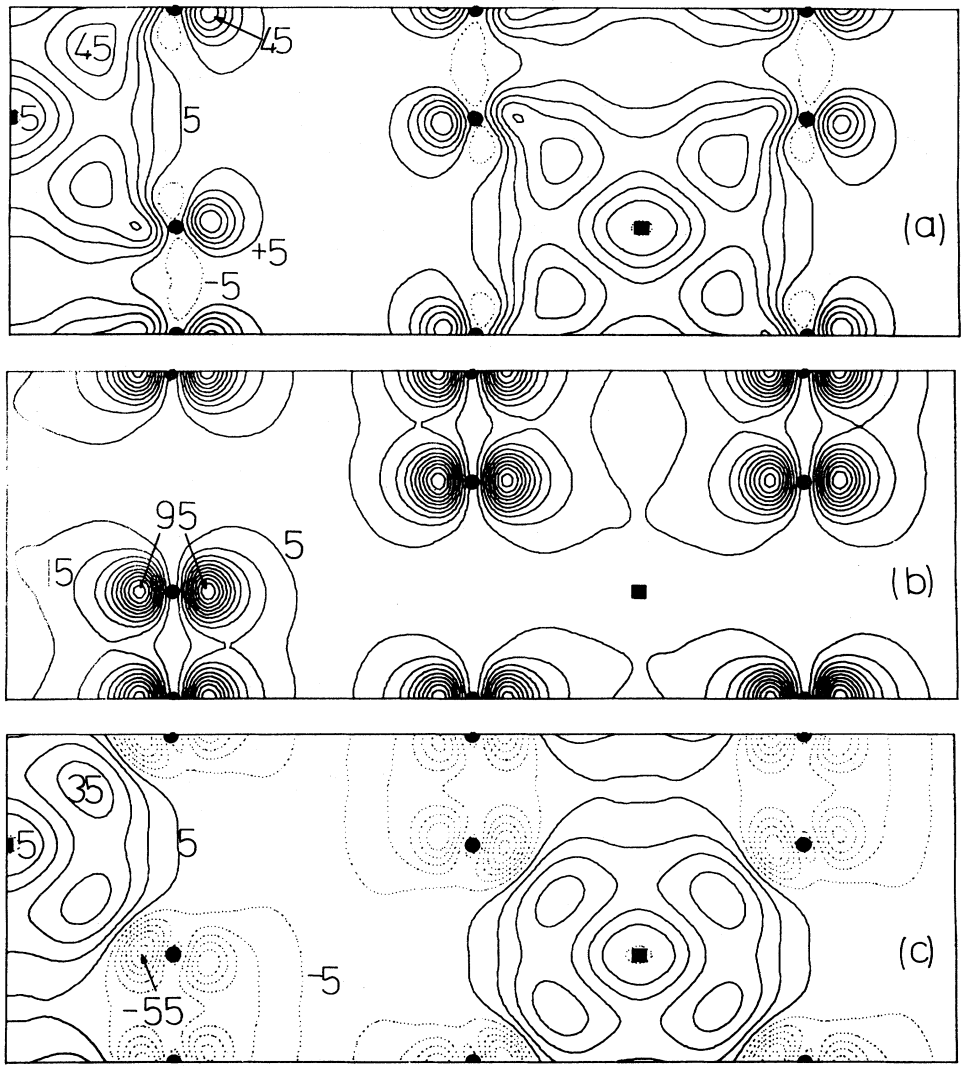

FIG. 6. Contour plots of electronic charge density of LiC_{12}: (a) total-difference density, (b) conduction-electron contribution, and (c) valence-electron contribution. Contour values are given in units of 0.001 electrons/Å^3. Atomic positions are denoted by filled squares for Li and circles for carbon. Plane shown is the same as in Fig. 3.

character in a layer plane, such as a partially antibonding graphite π state, is much smaller than the matrix element with a smooth wave function such as a bonding graphite π state. Hence, the conduction states of graphite are less polarizable than the valence states near the bottom of the π band. The valence-electron-difference density in Fig. 5(c), on the other hand, shows strong polarization effects; there exists a deficit of charge near the C planes and an excess of charge near the Li ions. From an analysis of the local density of states given below, we shall see that the valence-state polarization is not due only to states at the bottom of the π band, but also due to states spreading over a wide energy range.

The results of a similar charge-density analysis for LiC_{12} are shown in Fig. 6. Because of the reduced intercalant concentration and hence reduced charge transfer per carbon atom, the peak densities displayed in these plots for the second-stage compound are smaller than those for LiC_6 by roughly a factor of $\frac{1}{2}$. The polarization effects are exemplified by the asymmetry in the difference densities about each C site. As for the first-stage compound, the polarization effects on the conduction electrons [Fig. 6(b)] are very slight in comparison with that of the total- and valence-electron-difference densities.

The results for LiC_{18} are shown in Fig. 7. Near the bounding C layer and the Li plane, the total-electron-difference density [Fig. 7(a)] is strikingly similar to that of the second-stage compound shown in Fig. 6(a). Note that the difference density near the interior layer is small. However, the conduction-electron-difference contribution shown in Fig. 7(b) is much more delocalized. The valence-electron-difference density shown in Fig. 7(c) is also very similar in the region near the Li planes to that of the lower-stage compounds although the deficit region for

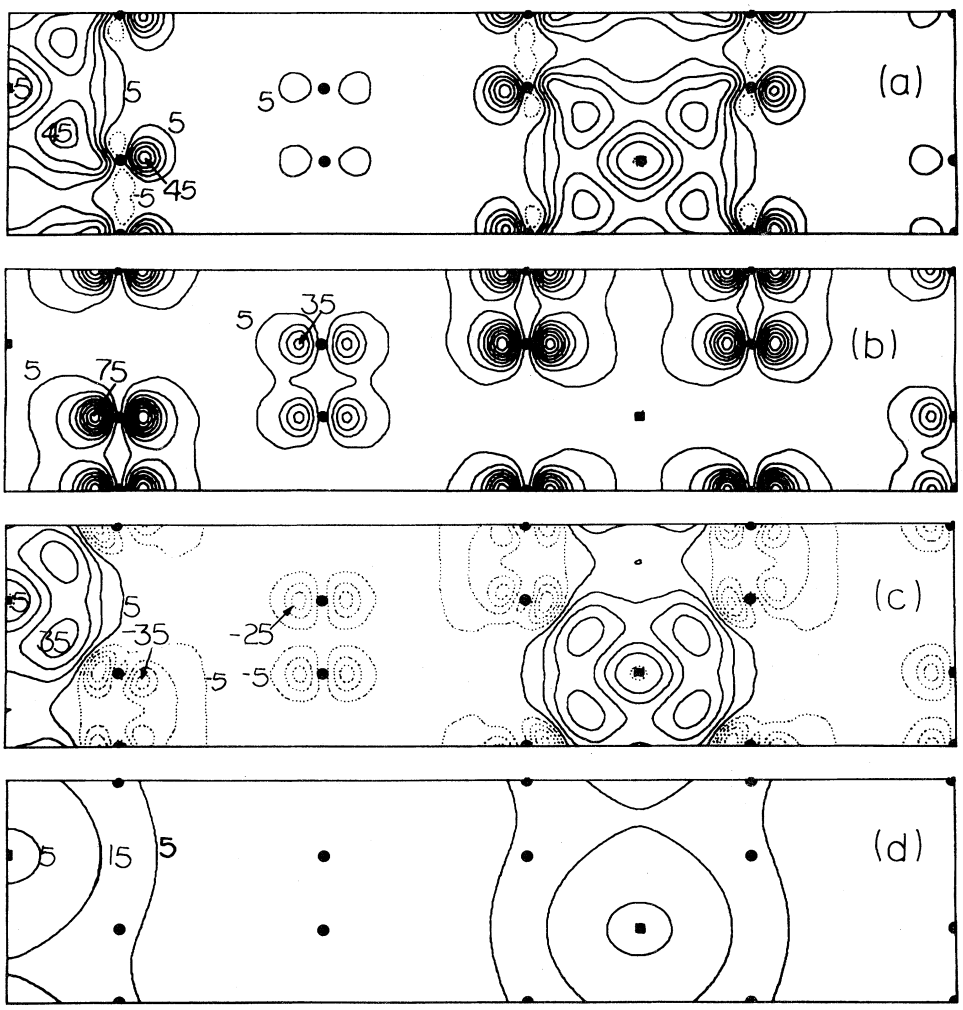

FIG. 7. Contour plots of electronic charge density for LiC_{18}: (a) total-difference density, (b) conduction-electron contribution, and (c) valence-electron contribution. Part (d) is a contour plot of superposed atomic charge density of Li 2*s* in the LiC_{18} structure. Contour values are given in units of 0.001 electrons/Å^3. Atomic positions are denoted by filled squares for Li and circles for carbon. Plane shown is the same as in Fig. 4.

LiC_{18} is more delocalized. In order to compare the polarization charge and that of a Li 2*s* bound-state density, the superposed density for atomic Li 2*s* states in the LiC_{18} structure is shown in Fig. 7(d). The polarization charge [Fig. 7(c)] retains some of its C character and therefore has more structure than that of the superposed atomic Li density. However, the similarity in the shapes of the two densities in Figs. 7(c) and 7(d) near the Li plane is apparent. In general the polarization charge is more localized near the Li ions than is the superposed charge, having a higher peak density in the Li plane at about 1 Å from each Li site and a lower density at the midpoint of the Li-Li separation.

An additional feature of the total-electron-difference density contour plots is the appearance of a deficit of charge in the region of the C—C bonds. In order to see the details of this effect, it is interesting to see the total-electron-difference density in some of the planes perpendicular to the planes presented in Figs. 5—7. Contour plots of the difference density in the Li plane and the bounding C-layer plane are shown in Fig. 8. The plot is for LiC_6, but the plots for the higher-stage compounds are very similar. The main difference is that, due to the reduced charge transfer per carbon atom, the contour levels in the bounding C-layer plane are lower in the higher-stage compounds by a factor of roughly $\frac{1}{2}$. The contour plot for the difference density in the Li-layer plane shown in the left-most panel of Fig. 8 is relatively structureless showing a saddle point in the difference density along a Li-Li nearest-neighbor distance—not indicative of a bond in the usual sense. The difference density in the C-layer plane shown in the right-most panel of Fig. 8 shows the withdrawal of electrons from the C—C bonds. There are two types of C—C bonds. The C—C bonds (type 1) in C hexagons with their center directly above or below a Li site suffer the greatest deficit while C—C bonds (type 2)

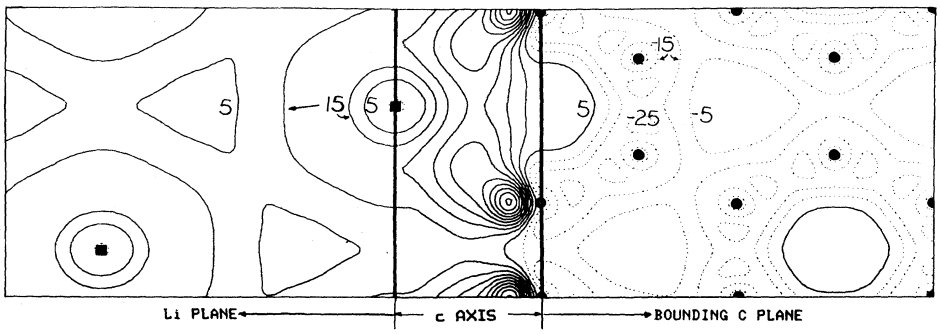

FIG. 8. Contour plot of total-difference density for LiC_6 shown in Li plane (left panel), plane of Fig. 5 (center panel), and in ("bounding") carbon-layer plane (right panel). The three planes intersect at 90° angles at the edges indicated by thick lines. Contour values are given in units of 0.001 electrons/Å^3. Atomic positions are denoted by filled squares for Li and circles for carbon.

which are further from the Li sites are affected less. This demonstrates the localized nature of the polarization. The withdrawal of charge from the C—C bond is quantified in Table II in terms of the integrated charge within a sphere centered on the various types of C—C bonds. For a sphere $\frac{1}{8}$th of the radius of the bond length, the charge with drawn from the type-1 bond is twice that withdrawn from the type-2 bond and 6 times that withdrawn from a bond in the interior layer of LiC_{18}. The percentages for LiC_{12} and the bounding layer of LiC_{18} are identical. The amount of charge withdrawal is small—a maximum of $\sim 1\%$ of the total, but this magnitude is large enough to affect the force constants and bond length of the C—C bond, for example. Our calculations were performed with an ideal structure—all C—C bonds having equal length. Although total energies and lattice relaxation were not included in the calculation, the results suggest that a structure with a slight dilation of the type-1 bonds relative to the type-2 bonds might have lower energy than the ideal structure. Such a structural effect of a distorted hexagonal structure within each bounding C plane could perhaps explain why the *AAαAA* stacking sequence (rather than *ABαBC* or *ABαBA*) occurs for LiC_{12}. That is, if registry of C atoms along the *c* axis is energetically more favorable for LiC_{12} in the presence of hexagonal distortion, only the *AAαAA* structure enables such registry.

TABLE II. Bond-charge changes. Percentage charge in carbon—carbon bonds of LiC_{6n} minus that of C_{6n} in sphere of radii $\frac{1}{4}$ and $\frac{1}{8}$ of the carbon—carbon bond length.

	$\frac{1}{4}$	$\frac{1}{8}$
LiC_6		
Bond 1[a]	−0.9%	−1.2%
Bond 2[b]	−0.5%	−0.6%
LiC_{12}		
Bond 1[a]	−0.4%	−0.6%
Bond 2[b]	−0.3%	−0.3%
LiC_{18}		
Bond 1[a]	−0.4%	−0.6%
Bond 2[b]	−0.3%	−0.3%
Bond 3[c]	−0.1%	−0.1%

[a]C—C bond in bounding layer in a C hexagon directly above or below a Li site.
[b]C—C bond in bounding layer in a C hexagon not directly above or below a Li site.
[c]C—C bond in interior layer.

In order to address the issue of charge transfer more quantitatively, it is helpful to look at the charge averaged in a layer plane and plotted along the *c* axis as shown in Figs. 9—11 for LiC_6, LiC_{12}, and LiC_{18}, respectively. The results of the linear plots follow the same trends shown in the contour plots as discussed above. Further, we can define regions *a*, *b*, and *c* as shown in these figures to compare the total integrated charge of the sandwich region, intermediate region, and interior region, respectively. The integrated charges for the three regions are listed in Table III. There are several interesting features of these results. First, the total-difference density in the sandwich region *a* is essentially the same in LiC_{12} and LiC_{18}, roughly 90% of the total excess charge. Secondly, the conduction-electron charge in regions *a* and *b* is nearly identical for both LiC_{12} and LiC_{18} indicating that the distortion polarization of the conduction states is small in contrast to that of the total-difference density. Thirdly, for LiC_{18}, roughly 20% of the conduction-electron charge is located in the interior layer, more than 3 times the charge of the total-difference density in this region.

One of the interesting questions remaining is to determine the origin of the charge density shown in the above results. This we can address by examining the local density of states of LiC_{18}. For this purpose, we have divided the crystal into the five regions *A*—*E* shown in Fig. 12(a). Region *A* is near the Li plane and is similar to region *D* if it were not for the Li atoms. Regions *B* and *C* are associated with the bounding carbon layer while region E is associated with the interior carbon layer. Comparing the local density of states for LiC_{18} in all of these regions (full line) with that of pure graphite in the LiC_{18} structure "C_{18}" (dashed line), for each region there is a strong similarity in the shape of the two curves. However, in each region there is an energy shift characteristic of an approximately two-dimensional electronic band structure modulated by the electrostatic potential in that region created by the charge transfer. The two curves have been aligned so that the bottom of the lowest-energy σ band is taken to be the zero of energy.

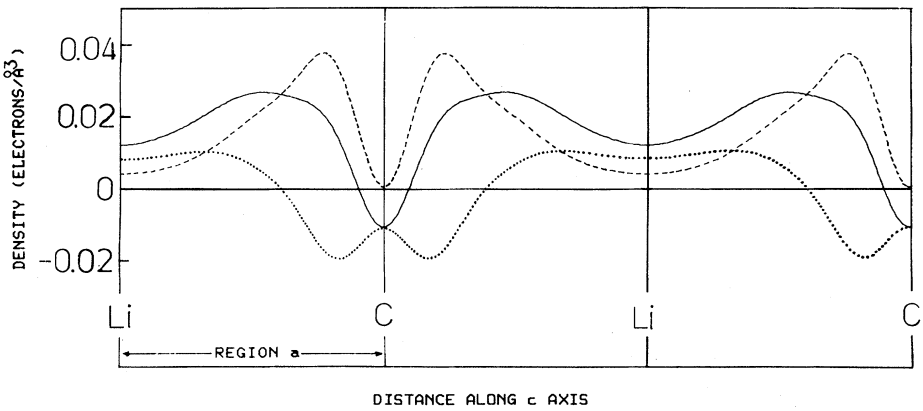

FIG. 9. Electronic charge densities for LiC_6 averaged in layer planes and plotted along c axis: total-difference density (full lines), conduction-electron contribution (dashed line), and valence-difference density (dotted line). Region definitions are those used in Table III.

The first interesting question is what is the origin of the charge near the Li plane? We can address this question by looking at the local density of states for region A in comparison to that for region D. Since these two regions are located between carbon planes, the main contribution to the occupied density in these regions is due to the π electrons whose band minimum is at roughly 12 eV. In region A the electrostatic potential for LiC_{18} shifts the energy levels to lower energies by approximately 0.5 eV. In region D the electrostatic potential of LiC_{18} shifts the energy levels to higher energies by approximately 0.5 eV. In addition to these rigid shifts there are some intensity differences between the graphite and LiC_{18} local-density-of-states curves. In region D, these differences are very small fluctuations throughout the region of occupied states, while in A systematic differences are apparent. Namely, the local density of states for LiC_{18} in region A for the occupied states is systematically higher than that of graphite especially for the bonding π bands in the region 12—18 eV. The density near the Li atoms is thus largely derived from the combined effects of the distortion of states in a 6-eV range of energy from the bottom of the π bands of graphite. The σ electrons also contribute to the polarization charge as evidenced by the bond-charge deficit shown in Fig. 8. However, because of their small extent into region A, their contribution is hardly visible in Fig. 12(a). A second interesting point illustrated in Figs. 12(a) and 12(b) is that states within roughly 1 eV on either side of the Fermi level of LiC_{18} have a local density of states whose shape is essentially identical to that of C_{18}. This result corroborates the arguments made above that the Fermi-level states are essentially unpolarizable.

A third point illustrated in Fig. 12(b) is the magnitude and sign of the electrostatic potential shifts associated with the bounding and interior carbon layers. To a first approximation, the local density of states (LDOS) of the interior layers (full curve E) is rigidly shifted by about 1 eV above the LDOS of the bounding layer (full curves B and C). In the region of the Fermi level, the electrostatic shift has been successfully modeled by several authors[25—28] who considered the effects of intercalation on the π bands of graphite alone.

Finally, the contribution of unoccupied Li $2s$ states is illustrated in Fig. 12(a) as enhancement in the local density of states of region A in the vicinity of 25 eV, several eV above E_F.

IV. RESULTS FOR BAND STRUCTURES

The band structure of LiC_6 is shown in Fig. 13 and is compared with previous calculations and experiment in Table IV. In general, the differences between the present

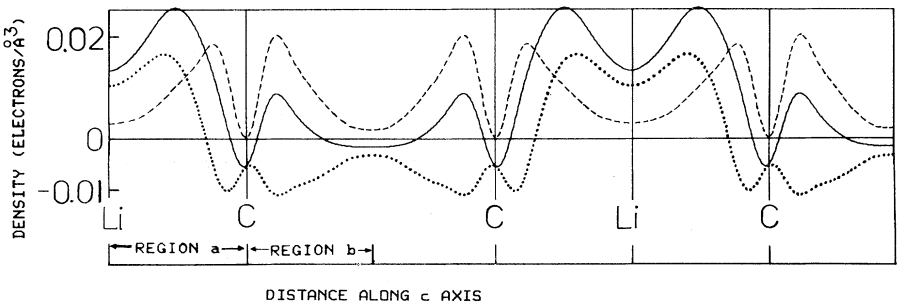

FIG. 10. Electronic charge densities for LiC_{12} averaged in layer planes and plotted along c axis: total-difference density (full lines), conduction-electron contribution (dashed line), and valence-difference density (dotted line). Region definitions are those used in Table III.

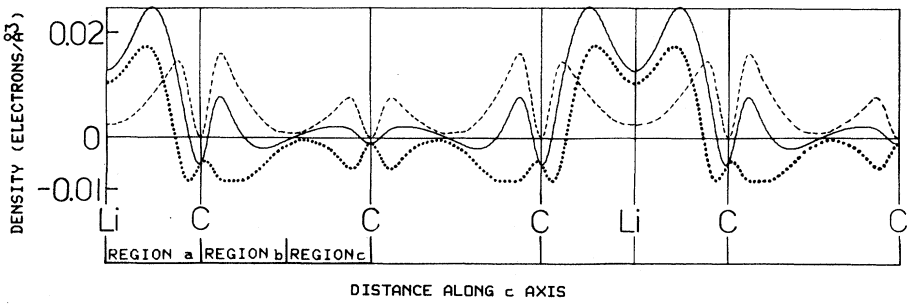

FIG. 11. Electronic charge densities for LiC_{18} averaged in layer planes and plotted along c axis: total-difference density (full lines), conduction-electron contribution (dashed line), and valence-difference density (dotted line). Region definitions are those used in Table III.

self-consistent band-structure results and the previous non-self-consistent results[14] follow the similar comparison for graphite itself.[2] The lower valence bands are in good agreement with the photoemission measurements.[24] The photoemission peak at 0.5 eV below the Fermi energy due to the "back-folded" π bands is perhaps related to the calculated bands at Γ; the corresponding states at A lie 1 eV or more lower in energy.

The band structures of LiC_{12} and LiC_{18} are shown in Figs. 14 and 15, respectively, along the symmetry directions defined in Table I. The general features of the bands are quite similar to those in LiC_6 except that there are 2 times as many and 3 times as many graphite bands for LiC_{12} and LiC_{18}, respectively, corresponding to the larger unit cells. By looking at the eigenfunctions one can distinguish states which are primarily localized on the bounding layers or on the interior layers for LiC_{18}. One finds that the interior-layer bands are raised in energy with respect to the corresponding levels of the bounding layers by roughly 1 eV. The magnitude of this electrostatic effect is comparable to the interlayer interaction of the π states as evidenced by the fact that the π-band splittings are only a few tenths of an eV larger for LiC_{18} than for LiC_{12}.

V. SUMMARY AND DISCUSSION

In summary, as a result of our study, we have learned about a number of properties of the model graphite intercalation compounds which we expect are generally applicable to this class of compounds.

(1) The total charge density of the intercalation compound screens the intercalant ion on a relatively short length scale. This is particularly evident in Table III where it is shown that 90% of the total-difference density of the second- and third-stage compounds is located in the sandwich region between two graphite layers surrounding a Li layer. This is also evidenced in Fig. 8 and Table II in terms of greater charge deficit from the C—C bond (type 1) closer to a Li ion. This total-charge-density distribution affects a number of ground-state properties such as the interlayer bond lengths[29] and force constants.[7,30] Evidence for the fact that the total-difference density is localized

TABLE III. Distribution of electronic charge in LiC_{6n}. Definitions of charge components and of regions are as defined for Figs. 9—11.

	Region a	Region b	Region c
LiC_6			
Total	0.50		
Conduction	0.50		
Valence	0		
LiC_{12}			
Total	0.45	0.05	
Conduction	0.26	0.24	
Valence	0.19	−0.19	
LiC_{18}			
Total	0.45	0.03	0.03
Conduction	0.21	0.19	0.09
Valence	0.23	−0.17	−0.07
Li $2s$			
Superposed atomic densities	0.40	0.09	0.01

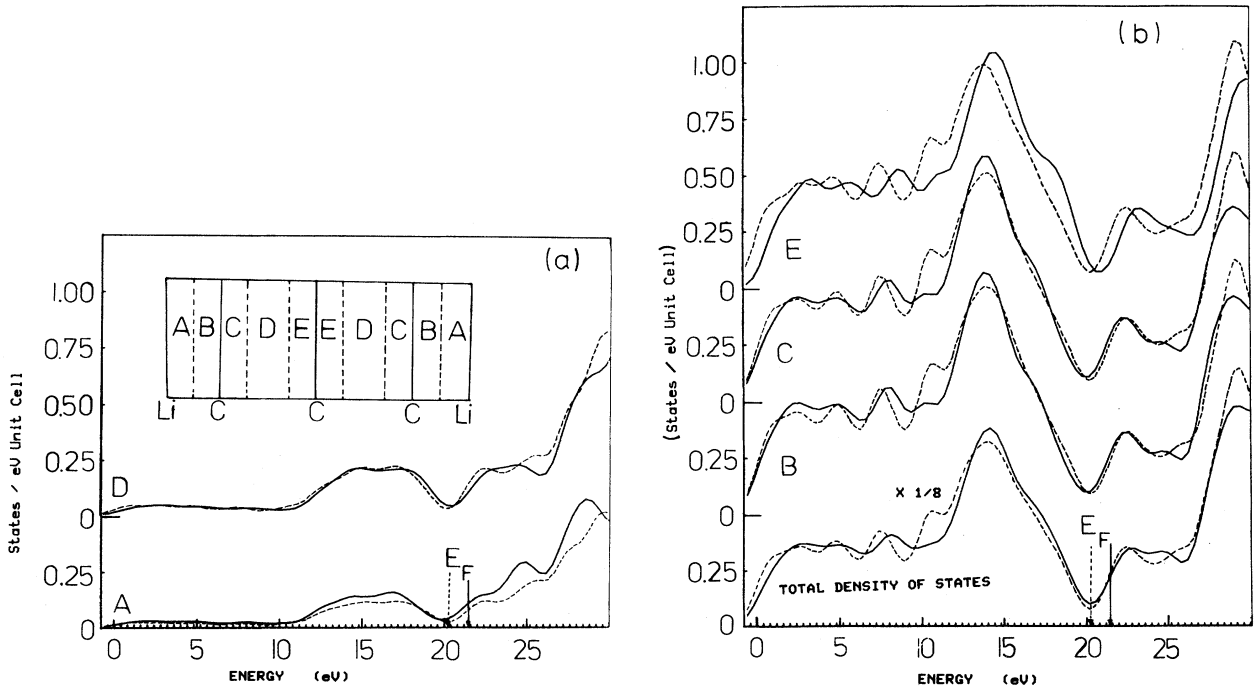

FIG. 12. Local density of states for LiC_{18} (full lines) and C_{18} (dashed lines). In (a) the inset is a diagram of the unit cell showing the division of regions $A-E$. Note that the volumes of $A-C$ and E are equal while D has a 60% larger volume. Sum of volumes $A+B+C+D+E$ is half that of a unit cell. In (a) the local density of states (LDOS) for region A (a bounding region between C planes near a Li plane) is compared with that of region D (an interior region between C planes). In (b) the LDOS for regions B and C (near a bounding C layer) and E (near an interior C layer) are compared with the total densities of states. Densities of states were obtained using histograms 0.4 eV wide smoothed with a Gaussian convolution function having a decay width of 1 eV.

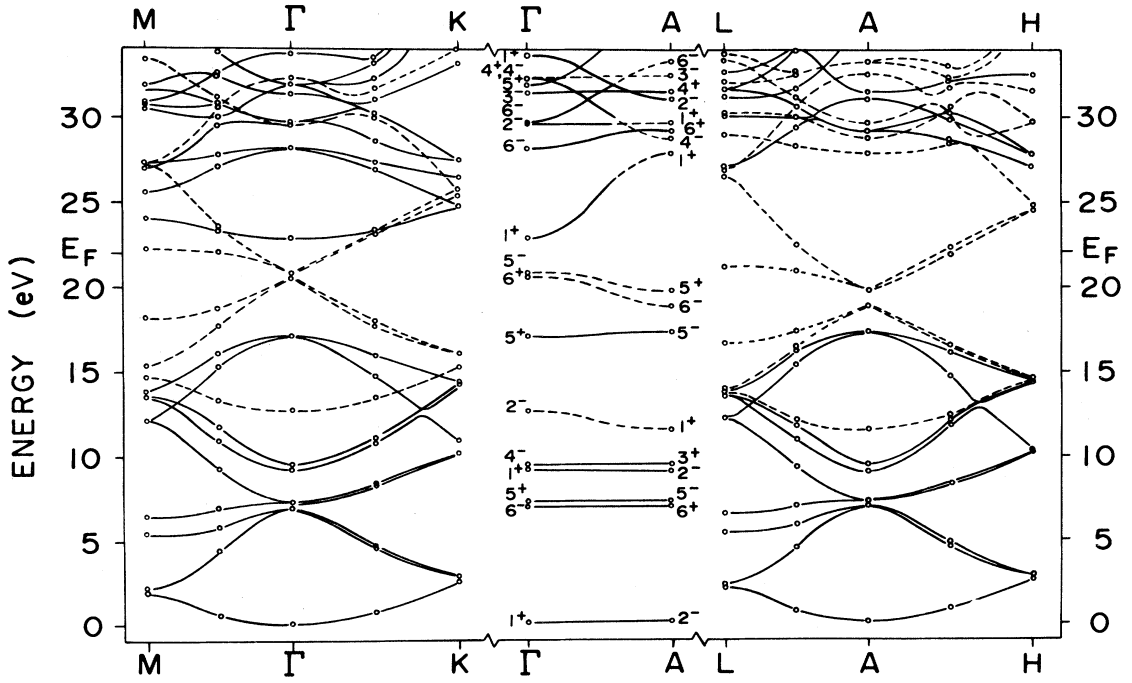

FIG. 13. Band structure of LiC_6. Dashed lines denote π bands; full lines denote σ bands. Energies calculated at points indicated by circles. Zero of energy taken at bottom of σ band. Notation for Brillouin zone and symmetry labels are the same as in Ref. 14. Brillouin-zone labels are also defined in Table I.

TABLE IV. Energy bands for LiC_6 in eV.

	Present results		Previous results[a]		Experiment[b]
	Γ	A	Γ	A	$\Gamma-A$
Bottom σ band[c]	0	0.2	0	−0.3	0
Back-folded σ bands	6.9	7.0	6.3	6.4	7.3
	7.3	7.3	6.8	6.7	
	9.2	9.1	8.4	8.0	9.5
	9.5	9.5	8.4	8.5	
Bottom π band	12.7	11.6	12.4	12.0	13.2
Top σ band	17.1	17.3	15.8	15.8	17.0
Back-folded π bands	20.6	18.8	20.1	19.4	22.0
	20.9	19.9	20.3	19.5	
E_F	21.6		21.8		22.5
"Metal" band	22.9	27.9	23.4	27.6	≈24.0[d]

[a]Reference 14.
[b]Reference 24. Experimental error quoted as ≤ 0.5 eV with respect to Fermi level.
[c]Bottom of σ band at Γ taken as zero of energy.
[d]From photoyield; level not necessarily at Γ.

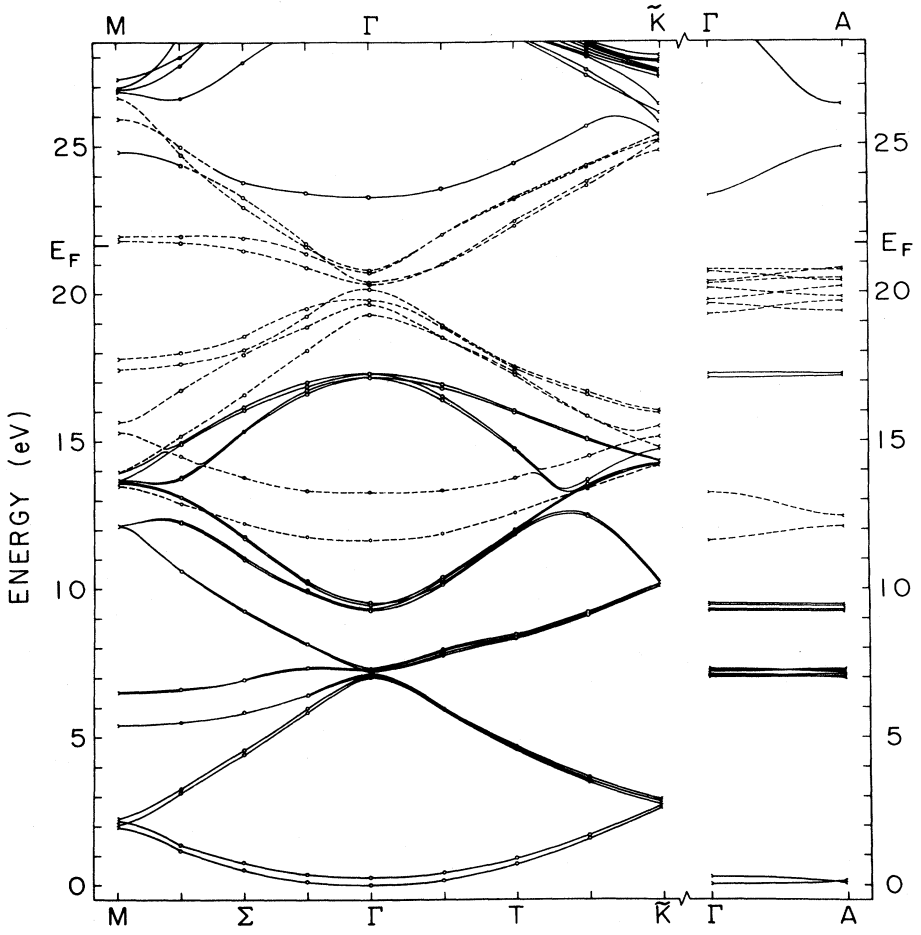

FIG. 14. Band structure of LiC_{12}. Dashed lines denote π band; full lines denote σ bands. Energies calculated at points indicated by circles. Zero of energy taken at bottom of σ band. Brillouin-zone labels are defined in Table I.

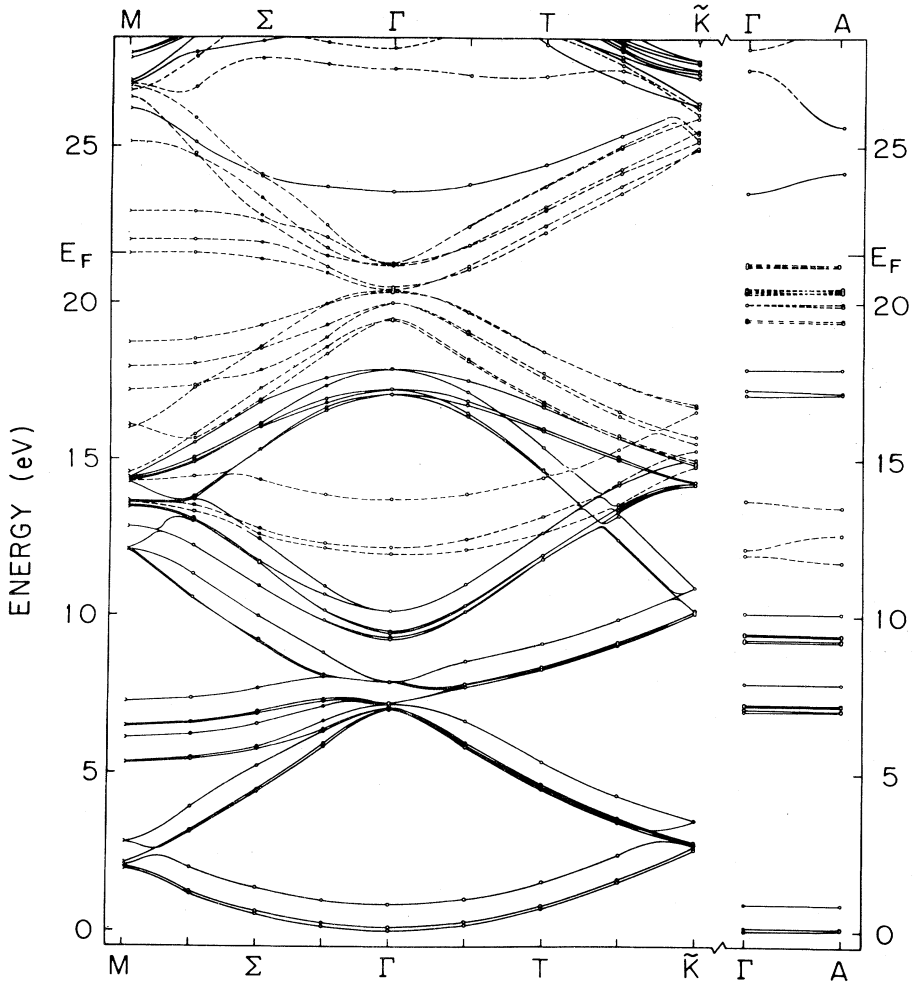

FIG. 15. Band structure of LiC_{18}. Dashed lines denote π bands; full lines denote σ bands. Energies calculated at points indicated by circles. Zero of energy taken at bottom of σ band. Brillouin-zone labels are defined in Table I.

near the Li ion has been suggested by the analysis of x-ray-photoemission measurements of the C 1*s* binding energies in a second-stage Li-intercalated graphite compound of presumed composition LiC_{18}.[31] The argument of the localized charge is based on the analysis of the linewidth to be consistent with four distinct C sites. If the difference density were more delocalized about the Li ion, there would be fewer distinct sites and a smaller linewidth. From the local density of states, we have, moreover, seen that the polarization charge is derived from the combined effects of a distortion of all the low-lying valence states of graphite. We have argued that this charge redistribution might result in a small lattice relaxation, lengthening the bonds closest to the Li ions and have cited the existence of the $AA\alpha AA$ stacking sequence for LiC_{12} as indirect evidence of this distortion effect.

(2) The conduction-electron contribution to the charge density is much more delocalized than the total-difference density and is virtually undistorted from a graphite π-like form. This is evidenced in Figs. 5(b), 6(b), and 7(b) as well as in Table III and in the form of the local density of states near the Fermi level as shown in Fig. 12. This behavior is due to the partly antibonding character of the states and has direct consequences in the transport[8,10] and Fermi-surface properties of graphite intercalation compounds. At the present time there is no direct evidence of the extent of the conduction-electron distribution. The most promising experimental tools for measuring this effect are the de Haas—van Alphen or Shubnikov—de Haas effects.[7] However, at the moment the results seem to be too sample dependent to be reliable.[32] The nondistortability of the π electrons near the Fermi level has been assumed in several successful model calculations[25–28] and is likely to be one of the major contributing factors to the high conductivity of the graphite intercalation compounds.

(3) Much of the physics of the electronic structure of the graphite intercalation compounds involves the manifold of the π states of graphite as shown by Safran and Hamann.[27] These authors were able to model the effects

of the σ electrons by a uniform dielectric constant. In fact, a comparison of the charge distribution predicted by such a model with that of the present results for the conduction electrons was quite reasonable.[33] However, not all of the effects of intercalation can be explained by such a model. The distribution of the total-difference density, the effects on the C—C bond, and the contribution to the polarization charge from the bonding π orbitals requires a more detailed treatment. The present results should help in the formulation of more sophisticated model calculations for more dilute intercalation compounds.

ACKNOWLEDGMENTS

We would like to thank J. E. Fischer, S. Safran, D. P. DiVincenzo, and R. C. Tatar for their helpful suggestions and stimulating discussions. A portion of this work was completed at the University of Pennsylvania supported by the National Science Foundation—Materials Research Laboratories program under Grant No. DMR-79-23647 and U.S. Army Research Office Contract No. DAAG-29-77-C400. One of us (S.G.L.) would like to acknowledge support from an Alfred P. Sloan Foundation Fellowship and National Science Foundation Grant No. DMR-78-22465.

---

*Present address: Department of Physics, City College of the City University of New York, Convent Avenue at 138th Street, New York, New York, 10031.

[1]N. A. W. Holzwarth, S. G. Louie, and S. Rabii, Phys. Rev. Lett. 47, 1318 (1982).

[2]N. A. W. Holzwarth, S. G. Louie, and S. Rabii, Phys. Rev. B 26, 5382 (1982); in Proceedings of the Symposium on the Local Density Approximations in Quantum Chemistry and Solid State Theory, Copenhagen, Denmark, June 11—12, 1982, edited by J. Avery and J. P. Dahl (in press).

[3]S. G. Louie, K.-M. Ho, and M. L. Cohen, Phys. Rev. B 19, 1774 (1979).

[4]D. R. Hamann, M. Schlüter, and C. Chiang, Phys. Rev. Lett. 43, 1494 (1979).

[5]L. Hedin and B. I. Lundqvist, J. Phys. C 4, 2064 (1971).

[6]R. Chen, P. Trucano, and R. F. Stewart, Acta Crystallogr. A 33, 823 (1977).

[7]For a comprehensive review, see, for example, M. S. Dresselhaus and G. Dresselhaus, Adv. Phys. 30, 139 (1981).

[8]D. Billaud, B. McRae, J. F. Mareche, and A. Hérold, Synth. Metals 3, 21 (1981).

[9]D. Guérard and A. Hérold, Carbon 13, 337 (1975).

[10]R. Juza and V. Wehle, Naturwissenschaften 52, 560 (1965).

[11]J. Rossat-Mignod, D. Fruchart, M. J. Moran, J. W. Milliken, and J. E. Fischer, Synth. Metals 2, 143 (1980).

[12]Capital letters denote graphite planes and Greek letters denote Li planes.

[13]N. Kambe, M. S. Dresselhaus, G. Dresselhaus, S. Basu, A. R. McGhie, and J. E. Fischer, Mater. Sci. Eng. 40, 1 (1979).

[14]N. A. W. Holzwarth, S. Rabii, and L. A. Girifalco, Phys. Rev. B 18, 5190 (1978).

[15]N. A. W. Holzwarth, L. A. Girifalco, and S. Rabii, Phys. Rev. B 18, 5206 (1978).

[16]S. Basu, C. Zeller, P. J. Flanders, C. D. Fuerst, W. D. Johnson, and J. E. Fischer, Mater. Sci. Eng. 38, 275 (1979).

[17]D. Billaud, E. McRae, and A. Herold, Mater. Res. Bull. 14, 857 (1979).

[18]J. E. Fischer, private communication; K. C. Woo, W. A. Kamitakahara, D. P. DiVincenzo, D. S. Robinson, H. Mertwoy, J. W. Milliken, and J. E. Fischer, Phys. Rev. Lett. 50, 182 (1983).

[19]D. E. Nixon, G. S. Parry, and A. R. Ubbelohde, Proc. R. Soc. London Ser. A 291, 324 (1966).

[20]D. E. Nixon and G. S. Pairy, Brit. J. Appl. Phys. (J. Phys. D) 1, 291 (1968).

[21]R. R. Haering, Can. J. Phys. 36, 352 (1958).

[22]J. W. McClure, Carbon 7, 425 (1969).

[23]J. D. Bernal, Proc. R. Soc. London Ser. A 106, 749 (1924).

[24]W. Eberhardt, I. T. McGovern, E. W. Plummer, and J. E. Fischer, Phys. Rev. Lett. 44, 200 (1980).

[25]L. Pietronero, S. Strässler, H. R. Zeller, and M. J. Rice, Phys. Rev. Lett. 41, 763 (1978); L. Pietronero, S. Strässler, and H. R. Zeller, Solid State Commun. 30, 305 (1979).

[26]S. A. Safran and D. R. Hamann, Phys. Rev. B 22, 606 (1980).

[27]S. A. Safran and D. R. Hamann, Phys. Rev. B 23, 565 (1981).

[28]J. Blinowsky and C. Rigaux, J. Phys. (Paris) 41, 667 (1980).

[29]L. Pietronero and S. Strässler, Phys. Rev. Lett. 47, 593 (1981).

[30]G. Dresselhaus and S. Y. Leung, Solid State Commun. 35, 819 (1980).

[31]S. B. DiCenzo, S. Basu and G. K. Wertheim, Synth. Metals 3, 139 (1981).

[32]The analysis of magneto-oscillatory data for graphite intercalation compounds is complicated by the appearance of extra signals and by the difficulty of detecting the high-frequency signal as has been recently pointed out by the detailed study of second-stage AsF_5-intercalated graphite by R. S. Markiewicz, H. R. Hart, Jr., L. V. Interrante, and J. S. Kasper, [Synth. Metals 2, 331 (1980)]; J. E. Fischer, M. J. Moran, J. W. Milliken, and A. Briggs, [Solid State Commun. 39, 439 (1981)].

[33]S. A. Safran, N. A. W. Holzwarth, and D. R. Hamann, in *Physics of Intercalation Compounds: Proceedings,* Vol. 38 of *Springer Series in Solid State Sciences, July, 1981, Trieste, Italy,* edited by L. Pietronero and E. Tosatti (Springer, New York, 1982).